Hindawi Publishing Corporation
Advances in Materials Science and Engineering
Volume 2016, Article ID 2821473, 9 pages
http://dx.doi.org/10.1155/2016/2821473

Research Article

Structural Stability and Dynamics of FGM Plates Using an Improved 8-ANS Finite Element

Weon-Tae Park

Division of Construction and Environmental Engineering, Kongju National University, 275 Budai, Cheonan 330-717, Republic of Korea

Correspondence should be addressed to Weon-Tae Park; pwtae@kongju.ac.kr

Received 22 April 2016; Accepted 7 June 2016

Academic Editor: Guillermo Rus

I investigate the vibration and buckling analysis of functionally graded material (FGM) structures, using a modified 8-node shell element. The properties of FGM vary continuously through the thickness direction according to the volume fraction of constituents defined by sigmoid function. The modified 8-ANS shell element has been employed to study the effect of power law index on dynamic analysis of FGM plates with various boundary conditions and buckling analysis under combined loads, and interaction curves of FGM plates are carried out. To overcome shear and membrane locking problems, the assumed natural strain method is employed. In order to validate and compare the finite element numerical solutions, the reference results of plates based on Navier's method, the series solutions of sigmoid FGM (S-FGM) plates are compared. Results of the present study show good agreement with the reference results. The solutions of vibration and buckling analysis are numerically illustrated in a number of tables and figures to show the influence of power law index, side-to-thickness ratio, aspect ratio, types of loads, and boundary conditions in FGM structures. This work is relevant to the simulation of wing surfaces, aircrafts, and box structures under various boundary conditions and loadings.

1. Introduction

Functionally graded material (FGM) is a special kind of composites in which the material properties vary continuously and smoothly from one surface to the other. One of the main advantages of FGM is that it mitigates acute stress concentrations and singularities at intersections between interfaces usually presented in laminated composites. Chung and Chi [1] proposed a sigmoid FGM, which is composed of two power law functions to define a new volume fraction and indicated that the use of a sigmoid FGM can significantly reduce the stress intensity factors of a cracked body. Recent work on the bending, vibration, buckling, and transient analysis of FGM plates can be founded in Han et al. [2, 3] and Jung and Han [4]. Recently, the works on FGM and shear deformation theories with the thickness stretching effect are employed and developed by researchers (Belabed et al. [5], Hamidi et al. [6], Lee et al. [7], and Han et al. [8]).

It should be noted that they only investigated structural behaviors of simply supported FGM plates. Thus, needs exist for the development of shell finite element which is simple to use for vibration and buckling analysis FGM plates with arbitrary boundary conditions.

When compressive loads are applied onto most structures including FGM plates, they tend to buckle or are subjected to dynamic loads during their operation. Understanding the natural frequency and buckling behavior is an important issue from design perspective. Consequently, numerous studies on vibration and buckling of various plates can be found in literatures. For proper use of FGM plates as various structural components, their dynamic and stability response should be studied. To the best of the author's knowledge, there are no solutions for structural stability response of FGM plates under combined compressive, tensile, and shear loads based on shear deformation theory of plate.

Bucalem and Bathe [9] improved the MITC8 shell elements [10] and concluded that while it performed quite effectively in some cases, in a few analyses the element presented a very stiff behavior rendering. In 8-node shell element [11, 12], the keeping of locking phenomena was found to continue through numerical solutions on the standard test problem of Macneal and Harder [13]. In order to improve the 8-node

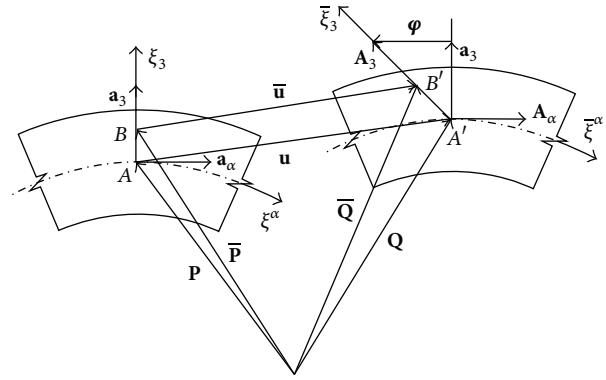

Figure 1: Kinematics of the first-order shear deformation theory.

ANS shell element, a new combination of sampling points is adopted. Recently, Han et al. [14] presented modified 8-ANS shell element using the new interpolation functions and combination of sampling points for the assumed natural strain.

However, a few literatures have been found on the dynamic analysis of FGM plates with various boundary conditions and structural stability analysis under combined compressive, tensile, and shear loads. In the present work modified 8-ANS shell element has been employed to study the effect of power law index on dynamic analysis of FGM plates with various boundary conditions and buckling analysis under combined compressive, tensile, and shear loads. To validate the present 8-ANS shell element models, the numerical examples are studied and compared with those results from the references. The solutions of vibration and buckling analysis are numerically illustrated in a number of tables and figures to show the influence of power law index, side-to-thickness ratio, aspect ratio, types of loads, and boundary conditions in FGM structures.

2. Modified 8-ANS Finite Element

2.1. Kinematics of Shell. The displacement $\bar{\mathbf{u}}$ of an arbitrary point of the shell (see Figure 1) for the first-order shear deformation theory can be expressed

$$\bar{\mathbf{u}}\left(\xi^\alpha\right) = \mathbf{u}\left(\xi^\alpha\right) + \xi_3 \boldsymbol{\varphi}\left(\xi^\alpha\right), \tag{1}$$

where $\boldsymbol{\varphi}$ is vector of rotation at the midsurface of shell.

A three-dimensional Green's strain tensor in the linear case (infinitesimal strain theory) is given by

$$2E_{ij} = \bar{\mathbf{u}}_{,i} \cdot \mathbf{g}_j + \bar{\mathbf{u}}_{,j} \cdot \mathbf{g}_i, \tag{2}$$

where a comma $(\,)_{,i} = \partial/\partial\xi^i$ is partial differentiation and $\mathbf{g}_i$ is a triad of base vectors for the spatial coordinates ξ^i at the surfaces (ξ_3 = const.) parallel to the midsurface of shell. If the displacement equation (1) is substituted into (2), the strain-displacement relations are obtained. From these strain-displacement relations, kinematics in different curvilinear coordinates can be acquired and expressed through the physical components in the matrix form

$$\mathbf{E} = \mathbf{B}\mathbf{U}, \tag{3}$$

where $\mathbf{U}$ are physical components of displacement $\mathbf{u}$ and rotation $\boldsymbol{\varphi}$ as follows:

$$\mathbf{U}^T = \left[u_1, u_2, u_3, \phi_1, \phi_2, \phi_3\right]. \tag{4}$$

The shell theory presented above is the so-called first-order shear deformation theory with six degrees of freedom.

2.2. Various Enhanced Strain Interpolation Patterns. In this study, the ordinary 8 nodes of Lagrangian displacement interpolations are used and the various combinations of assumed natural strain interpolation functions are employed for the very efficient 8-node shell element. Figure 2 shows various patterns of sampling points that can be used for membrane, in-plane shear, and out-of-plane shear strain interpolations for the new 8-ANS finite element. Based on Figure 2, the β pattern is used for membrane and the δ pattern and γ_6^* pattern are used for in-plane and out-of-plane shear, respectively. The interpolation functions by Polit et al. [16] are used in the γ_6^* patterns. In the γ_6^* patterns, the strain component of center point is replaced by the mean of the components at points S_1 and S_2 (Bathe and Dvorkin, [10]).

3. Material Properties of the FGM

An FGM can be defined by the variation in the volume fractions. In this paper, the sigmoid function is used for FGM structures. The volume fraction using two power law functions which confirm smooth distribution of stresses is defined by

$$V_f^1(t) = 1 - \frac{1}{2}\left(\frac{h/2 - t}{h/2}\right)^p \quad \text{for } 0 \le t \le \frac{h}{2}, \tag{5a}$$

$$V_f^2(t) = \frac{1}{2}\left(\frac{h/2 + t}{h/2}\right)^p \quad \text{for } -\frac{h}{2} \le t \le 0, \tag{5b}$$

where subscripts 1 and 2 represent the two materials used and p is the power law index, which indicates the material variation profile through the thickness. The material properties

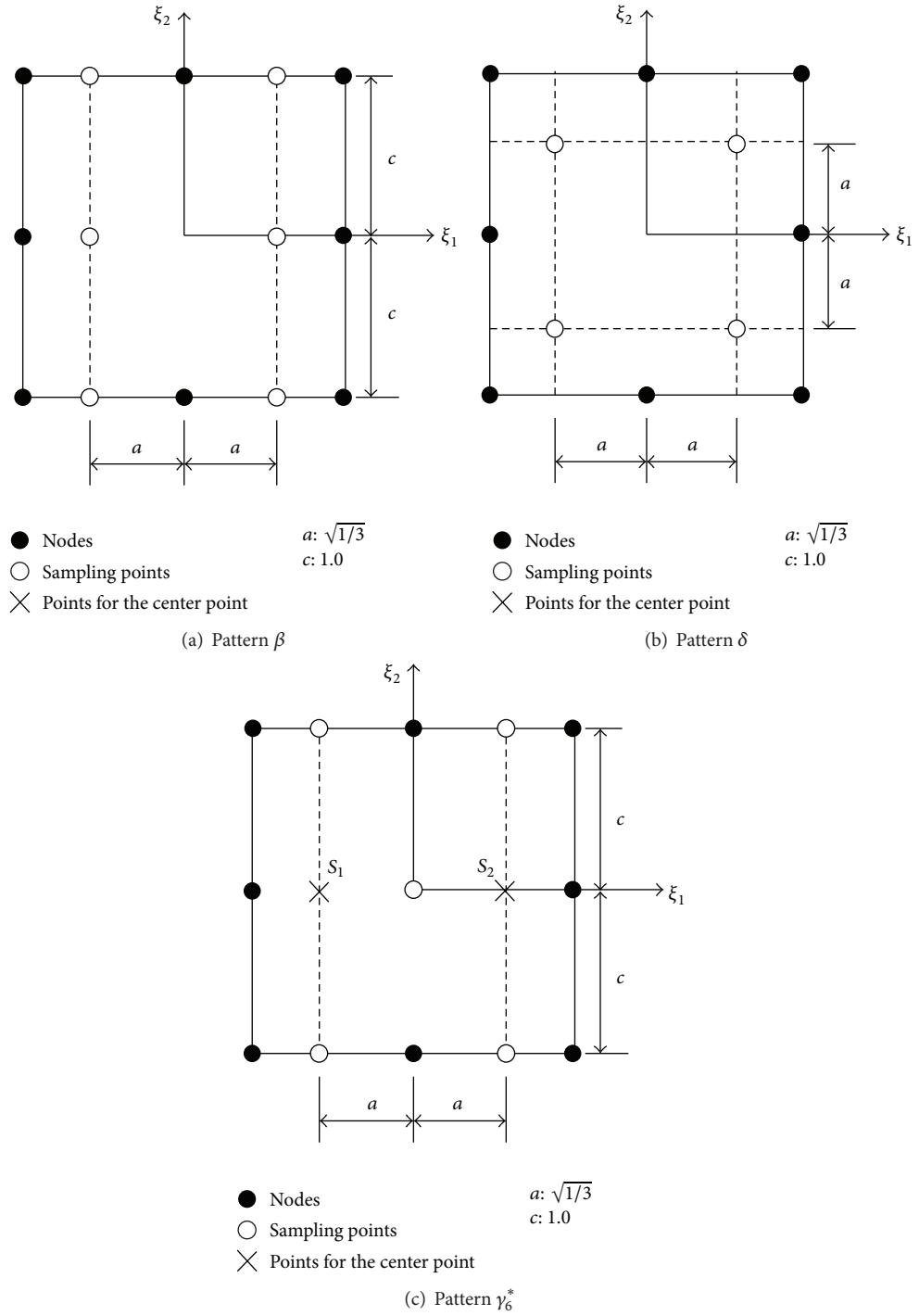

Figure 2: Four possible patterns of sampling points for 8-node ANS shell element.

of the S-FGM using the rule of mixture can be expressed as follows:

$$H(t) = V_f^1(t) H_1 + \left(1 - V_f^1(t)\right) H_2 \quad \text{for } 0 \le t \le \frac{h}{2}, \tag{6a}$$

$$H(t) = V_f^2(t) H_1 + \left(1 - V_f^2(t)\right) H_2 \quad \text{for } -\frac{h}{2} \le t \le 0. \tag{6b}$$

4. Equilibrium Equation

By using virtual work principle, the equilibrium equation is obtained based on the membrane (**N**), bending (**M**), and transverse shear resultant forces (**Q**) as follows:

$$\int \left(\delta \left(E_{\alpha\beta}^m\right)^T \mathbf{N} + \delta \left(E_{\alpha\beta}^b\right)^T \mathbf{M} + \delta \left(E_{\alpha 3}^s\right)^T \mathbf{Q}\right) dA \equiv \delta \mathbf{u}^T \mathbf{K}_L \mathbf{u} = \int \mathbf{f} \cdot \delta \mathbf{u}\, dV, \tag{7}$$

Table 1: Results of patch test under bending, shear, and tension.

Patch tests	Bending	Shear	Tension
Reference solutions	$\theta_y = \frac{ML}{EI} = 0.12 \times 10^{-4}$	$w = \frac{6SL}{5GA} = 0.312 \times 10^{-5}$	$u = \frac{TL}{EA} = 1.0 \times 10^{-6}$
Normalized solutions	1.000	1.000	0.992

where $E^m_{\alpha\beta}$, $E^b_{\alpha\beta}$, and $E^s_{\alpha 3}$ are membrane, bending, and transverse shear strain components, $\mathbf{K}_L$ is the linear stiffness matrix, and $\mathbf{f}$ is the body force.

5. Buckling and Vibration Analysis

When the equation is employed to estimate buckling loads, the stability condition may be simplified by

$$\mathbf{K}_L \mathbf{u}^a + \lambda_{\text{cr}} \mathbb{G} \mathbf{u}^a = 0, \tag{8}$$

where $\mathbf{u}^a$ is the vector of the nodal value of the displacements, λ_{cr} is the buckling load parameter and denotes the proportional increase in load needed to reach neutral equilibrium, and $\mathbb{G}$ is the geometric stiffness matrix. Applying to the structure a reference loading N_{ref} and carrying out a generalized linear static analysis, (8) represents the standard eigenvalue problem. The lowest eigenvalue λ_{cr} in (8) is associated with buckling load. Therefore, the buckling load can be obtained by

$$N_{\text{cr}} = \lambda_{\text{cr}} N_{\text{ref}}. \tag{9}$$

The consistent mass is used to formulate the mass matrices for the FGM shell element. The mass matrix is determined using interpolation functions as follows:

$$M = \int_V \rho N^T N \, dV, \tag{10}$$

where N is a matrix of shape functions.

Unlike (8), the governing equations of motion for free vibration analysis are of the form

$$\mathbf{K}_L \mathbf{u}^a + M \ddot{\mathbf{u}}^a = 0, \tag{11}$$

where the superposed dot denotes differentiation with respect to time.

6. Numerical Results

6.1. Patch Test. Firstly, the patch tests proposed by Simo et al. [15] are investigated. In Figure 3, the boundary conditions and loading types are presented, simultaneously. The normalized solutions of nodal displacements on the right edges are shown in Table 1. The nondimensional form is expressed as follows:

$$\text{Normalized solution} = \frac{\text{Present solution}}{\text{Reference solution}}. \tag{12}$$

6.2. Vibration Analysis

6.2.1. Simply Supported Rectangular FGM Plate. To validate the present 8-ANS finite element with FGM, a sigmoid FGM plate with geometrical properties is shown in Figure 4. The material properties are given by

$$\begin{aligned} E_1 &= 151 \times 10^9 \text{ Pa}, \\ \rho_1 &= 3000 \text{ kg/m}^3, \\ E_2 &= 70 \times 10^9 \text{ Pa}, \\ \rho_2 &= 2707 \text{ kg/m}^3, \\ \nu_1 &= \nu_2 = 0.3, \end{aligned} \tag{13}$$

where E_1, ρ_1, ν_1 and E_2, ρ_2, ν_2 express the property of the top and bottom faces of the plate, respectively. Equation (13) is used in computing the numerical values of all cases.

The nondimensional form of the results is defined by

$$\overline{\omega} = \omega \left(\frac{a^2}{h} \sqrt{\frac{\rho_1}{E_2}} \right). \tag{14}$$

Table 2 shows the nondimensional natural frequency of S-FGM simply supported plates for convergence test. It is noticed that present 8-ANS finite element shows an excellent agreement to the result by analytical solution.

It is shown that the natural frequency of pure metal plate is smaller than that of pure ceramic plate in Table 3. The natural frequencies of the functionally graded material plates are intermediate to that of the metal and ceramic plates. Table 3 shows that numerical results of vibration analysis are reduced by increasing the power law p.

Table 4 shows the numerical results of FGM plate for which $p = 10$. In this example, the natural frequency is normalized with respect to the plate width a, thickness h, density ρ_1, and elastic modulus E_2 for various rectangular plate aspect ratios. As the plate aspect ratio increases, the natural frequency reduces and approaches 3.69.

6.2.2. FGM Plate with Arbitrary Edges. For convenience, a four-letter notation is used to describe the boundary conditions of the edges (see Figure 5). For example, CFSF indicates that first edge is clamped (C), second edge is free (F), third edge is simply supported (S), and the last is free (F). The natural frequencies of FGM CFFF plates are investigated and presented in Table 5. The results are expressed in the nondimensional form using (15). Numerical results show that the natural frequencies are reduced by increasing the power

Table 2: Normalized nondimensional natural frequency of S-FGM plate (power law index: $p = 10$).

Nodes per side	4-node shell element (see [2])[b]	Ratio ([2]/exact)	Present	Ratio (present/exact)
5	8.076	1.105	7.717	1.056
9	7.517	1.029	7.351	1.006
17	7.366	1.008	7.323	1.002
33	7.329	1.003	—	—
Analytical solution[a]	7.307	—	—	—

[a]Result is computed using Navier's method with first-order shear deformation theory, independently.
[b]Results are computed using the quasi-conforming 4-ANS finite element, independently.

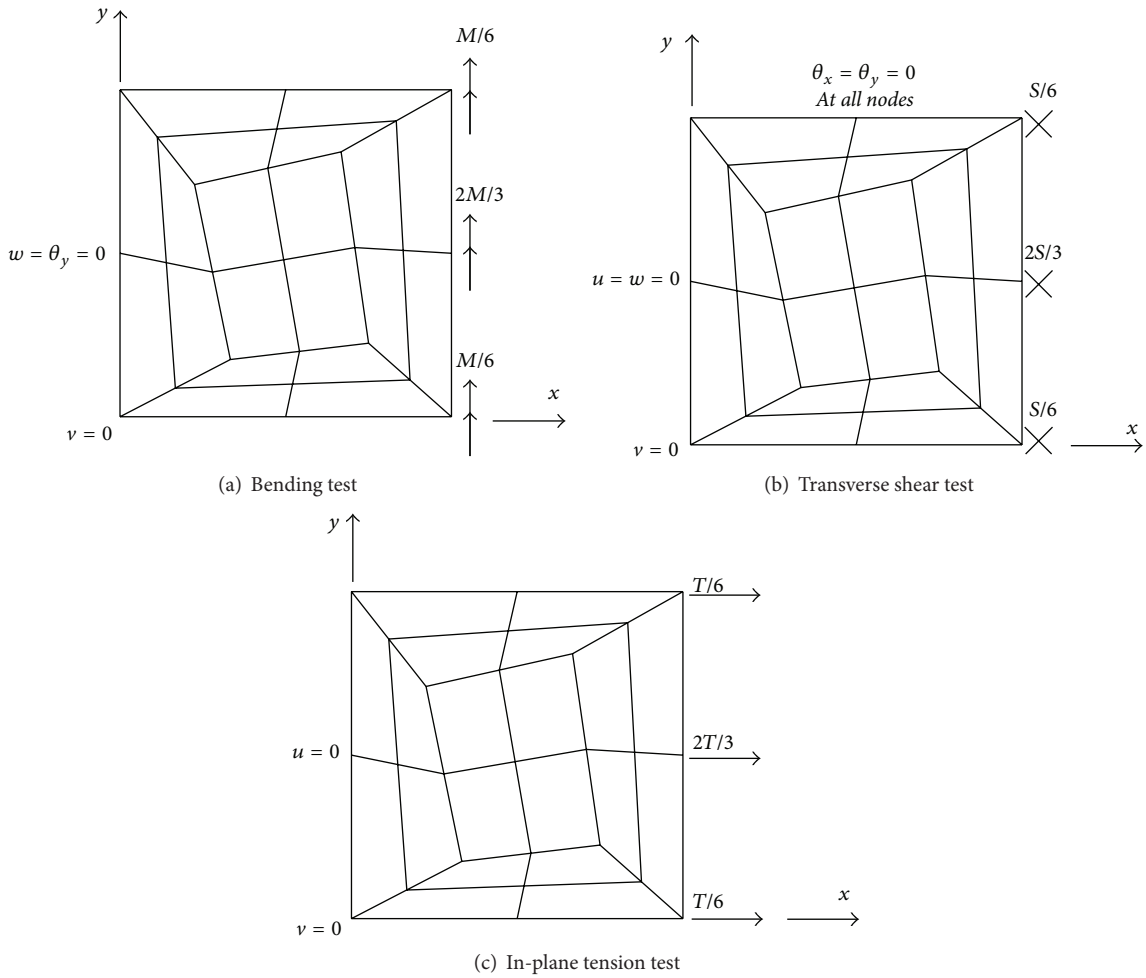

Figure 3: Mesh for patch test (Simo et al. [15]). Length of the square $L = 10$; Young's modulus $E = 1.0 \times 10^7$; Poisson's ratio $\nu = 0.3$; and thickness $h = 1.0$ and boundary displacement conditions for patch tests.

law index p. The results also confirm that power law index has significant effect on the dynamic response of FGM plates:

$$\overline{\omega} = \omega \left(\frac{a^2}{h} \sqrt{\frac{\rho_1}{E_2}} \right) \times 10. \tag{15}$$

In Table 6, the natural frequencies of FGM plates with arbitrary boundary conditions are presented. Four arbitrary values of the power law index p are examined. As expected, results show that the natural frequencies are reduced by increasing the power law index p.

Based on present study, comprehensive results of natural frequency of FGM plates are also illustrated in Figure 7 for different boundary conditions. In each boundary condition, five different power law indices are considered. In Figure 8, two different values of side-to-thickness ratio are examined. In addition, five arbitrary values of the power law index are examined. These new results can be used for comparison with further FG plate models.

Table 3: Nondimensional natural frequency of simply supported FGM plates ($a/h = 100$).

Material parameter (p)	Navier solution	Mode number 1		2		3	
		Ref. [2]	Present	Ref. [2]	Present	Ref. [2]	Present
Pure ceramic	8.992[a]	9.041[a]	8.772	22.705[a]	21.940	22.705[a]	21.940
$p = 1$	7.518	7.555	7.526	18.992	18.819	18.993	18.820
$p = 2$	7.419	7.457	7.430	18.745	18.575	18.747	18.576
$p = 5$	7.333	7.373	7.348	18.533	18.365	18.535	18.367
$p = 10$	7.307	7.348	7.323	18.470	18.302	18.472	18.304
Pure metal	6.123[a]	6.148[a]	6.287	15.459[a]	15.726	15.459[a]	15.726

[a]Results are calculated by $\rho = (\rho_1 + \rho_2)/2$.

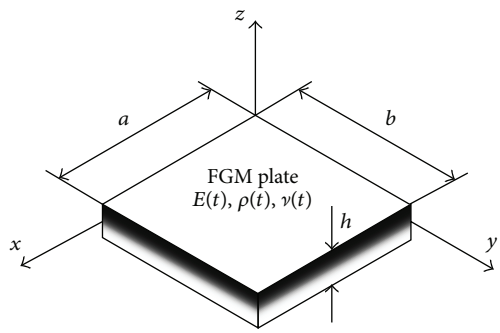

Figure 4: Geometry of FGM plates.

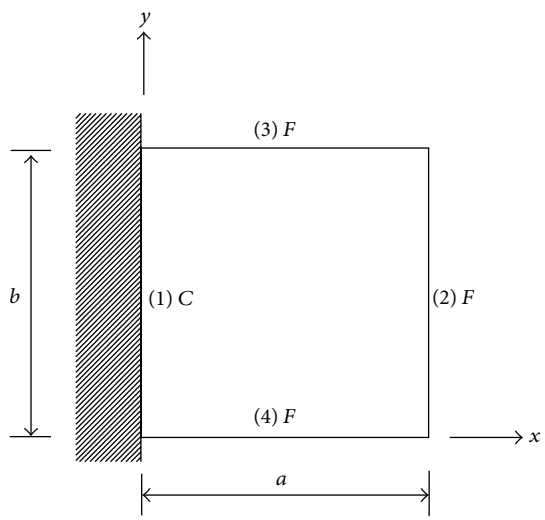

Figure 5: Geometry of FGM cantilever plates.

Table 4: Nondimensional fundamental frequency of simply supported FGM plates with various aspect ratio ($p = 10$).

Solutions	Aspect ratio (b/a)			
	0.5	2.0	5.0	10.0
Navier solution	18.258	4.568	3.800	3.691
Ref. [2]	18.346	4.593	3.817	3.706
Present	18.276	4.577	3.803	3.692

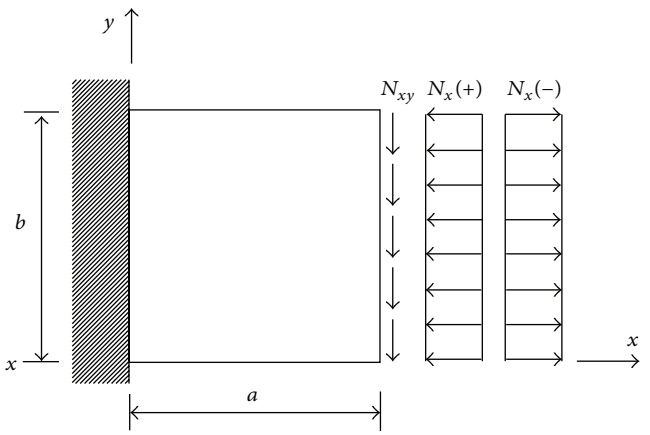

Figure 6: FGM cantilever plates under combined loads.

6.3. Buckling Analysis

6.3.1. Simply Supported Rectangular FGM Plate. For validation, the stability analysis results of S-FGM simply supported plates (see Figure 4) using Navier's method are compared with present 8-ANS finite element. The material properties and nondimensional form are used as shown in Section 6.2.1 and (14), respectively. It is shown that the pure ceramic plate has the largest buckling load and the pure metal plate has the smallest one in Table 7. The buckling loads of the FGM plates are intermediate to that of the metal and ceramic plates.

The buckling loads versus the plate aspect ratio are presented in Table 8. There, for large plate aspect ratios (i.e., $b/a \geq 2.0$), the plate buckles into a single half wave in the x-direction. As the plate aspect ratio decreases, the plate buckles with increasing half waves in the x-direction.

6.3.2. FGM Cantilever Plate. In Table 9, the stability analysis results of S-FGM cantilever plates (see Figure 6) with various aspect ratio are presented. The results are presented in the nondimensional form. Numerical results show that the buckling loads are reduced by increasing the power law index p. The results also confirm that power law index has significant effect on the buckling loads of FGM cantilever plates. The stability analysis results of S-FGM cantilever plates

Table 5: Nondimensional natural frequency of FGM CFFF plates ($a/h = 100$).

Material parameter (p)	Mode number 1		2		3		4	
	Ref. [2]	Present	Ref. [2]	Present	Ref. [2]	Present	Ref. [2]	Present
Pure ceramic	15.814[a]	15.430	38.767[a]	37.780	97.148[a]	94.570	124.28[a]	120.80
$p = 1$	13.222	13.228	32.415	32.389	81.236	81.074	103.92	103.56
$p = 2$	13.047	13.052	31.986	31.960	80.166	80.000	102.54	102.19
$p = 5$	12.896	12.901	31.617	31.590	79.244	79.073	101.36	101.00
$p = 10$	12.851	12.856	31.507	31.480	78.969	78.797	101.01	100.65
Pure metal	10.767[a]	11.060	26.395[a]	27.079	66.144[a]	67.785	84.615[a]	86.584

[a]Results of [2] are calculated by $\rho = (\rho_1 + \rho_2)/2$.

Table 6: Nondimensional natural frequency of FGM plates ($a/h = 100$).

Material parameter (p)	Boundary conditions				
	CFFF	SSFF	SSSS	CCFF	CCSS
Pure ceramic	15.430	54.302	87.718	98.502	128.59
$p = 1$	13.228	46.643	75.264	84.446	110.25
$p = 2$	13.052	46.078	74.304	83.327	108.79
$p = 5$	12.901	45.591	73.478	82.364	107.53
$p = 10$	12.856	45.446	73.231	82.077	107.15
Pure metal	11.060	38.922	62.873	70.603	92.176

Table 7: Nondimensional buckling loads of FGM simply supported plates ($\overline{N}_{cr} = N_{cr}b^2/E_2h^3$).

Material parameter (p)	Navier solution	Ref. [2]	Present
Pure ceramic	7.794	7.828	7.797
$p = 1$	5.448	5.484	5.466
$p = 2$	5.305	5.346	5.331
$p = 5$	5.183	5.229	5.216
$p = 10$	5.147	5.195	5.182
Pure metal	3.613	3.629	3.615

Table 8: Nondimensional buckling loads of FGM simply supported plates ($\overline{N}_{cr} = N_{cr}b^2/E_2h^3$, $p = 10$).

Solutions	Aspect ratio (b/a)			
	0.5	2.0	5.0	10.0
Navier solution	5.138	8.043	34.800	131.28
Ref. [2]	5.211	8.127	34.969	131.87
Present	5.165	8.110	34.859	131.37

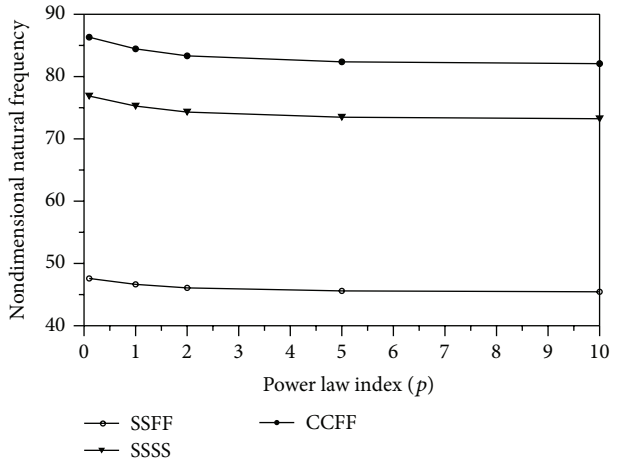

Figure 7: Effect of power law index on the nondimensional natural frequency of FGM plate with arbitrary edges.

under various loading types are investigated in Table 10. As expected, numerical results show that the buckling loads are reduced by increasing the power law index p and also confirm that loading types have very significant effect on the buckling loads of FGM cantilever plates.

Based on present study, comprehensive results of buckling loads of FGM plates under combined loads are also illustrated in Figures 9 and 10 for CFFF boundary conditions. The influence of in-plane load direction on the relationship between critical shear and in-plane loading is studied, when acting in combination. It is noticed that the tension may produce positive stiffness and the FGM plate becomes stronger than when it is subjected to compression.

In Figure 10, the natural frequencies of FGM plates under combined loading are investigated. Four arbitrary values of the power law index p are examined. As expected, results show that the buckling loads are increased by decreasing the power law index p.

Table 9: Nondimensional buckling loads of FGM plates ($\overline{N}_{cr} = (N_{cr}b^2/E_2h^3) \times 10$).

Material parameter (p)	Aspect ratio (b/a)							
	1		2		5		10	
	Ref. [2]	Present	Ref. [2]*	Present	Ref. [2]*	Present	Ref. [2]*	Present
Pure ceramic	4.693	4.679	9.551	19.040	24.160	120.75	48.449	485.42
$p = 1$	3.281	3.271	6.677	13.310	16.890	84.411	33.872	339.32
$p = 2$	3.194	3.185	6.501	12.959	16.445	82.185	32.981	330.38
$p = 5$	3.121	3.111	6.351	12.660	16.067	80.293	32.224	322.77
$p = 10$	3.099	3.090	6.307	12.572	15.955	79.733	32.000	320.52
Pure metal	2.176	2.169	4.428	8.8265	11.200	55.979	22.460	225.03

*Results of [2] are calculated by $\overline{N}_{cr} = (N_{cr}a^2/E_2h^3)(b/a) \times 10$.

Table 10: Nondimensional buckling loads of FGM plates ($\overline{N}_{cr} = (N_{cr}b^2/E_2h^3) \times 10$).

Material parameter (p)	Types of combined loading			
	Compression	Shear + comp.	Pure shear	Shear + tension
	Present	Present	Present	Present
Pure ceramic	4.679	4.279	15.135	95.116
$p = 1$	3.271	2.991	10.580	66.495
$p = 2$	3.185	2.912	10.302	64.745
$p = 5$	3.111	2.845	10.065	63.257
$p = 10$	3.090	2.826	9.9946	62.816
Pure metal	2.169	1.984	7.0163	44.094

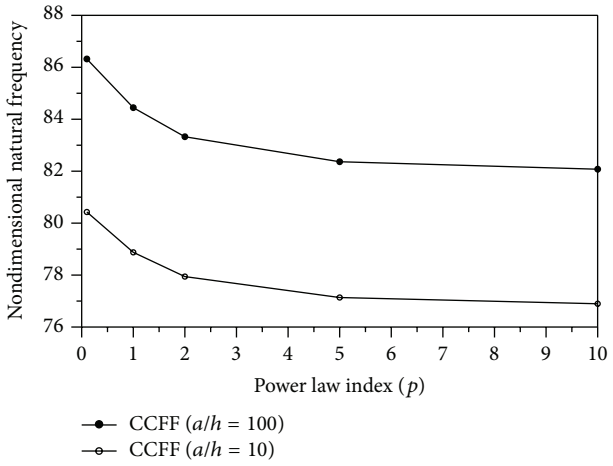

Figure 8: Effect of power law index on the nondimensional natural frequency of CCFF FGM plate with variation of side-to-thickness ratio.

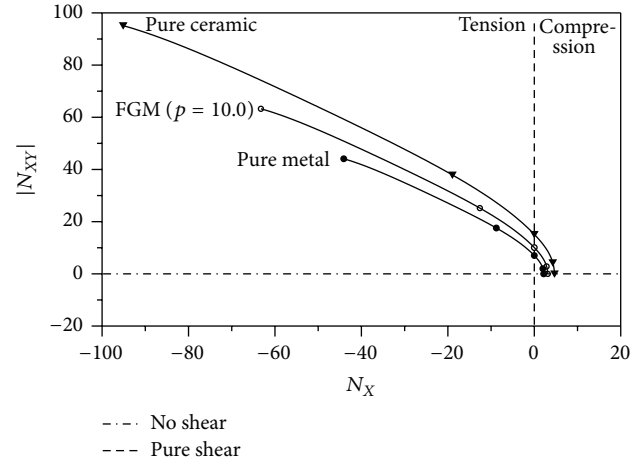

Figure 9: Buckling load of FGM plates: combined compressive, tensile, and shear loading.

7. Concluding Remarks

The natural frequency and buckling response have been studied for FGM plates. Extensive results obtained from computations refer to different loading, different geometry, different boundaries, and different power law indices. The advanced finite element analysis based on the modified 8-node ANS formulation shows the significance of various boundary conditions and loading conditions for FGM plates. From this study, a number of conclusions have been founded.

(1) It is shown that the natural frequencies are reduced by increasing the power law index p. The results also confirm that power law index has significant effect on the dynamic response of FGM plates.

(2) Dynamic response of FGM plates is affected by its boundary conditions. Clamped edges always produce a higher performance of the FGM plates than simply supported edges.

(3) It is noticed that the tension may produce positive stiffness and the FGM plate becomes stronger than

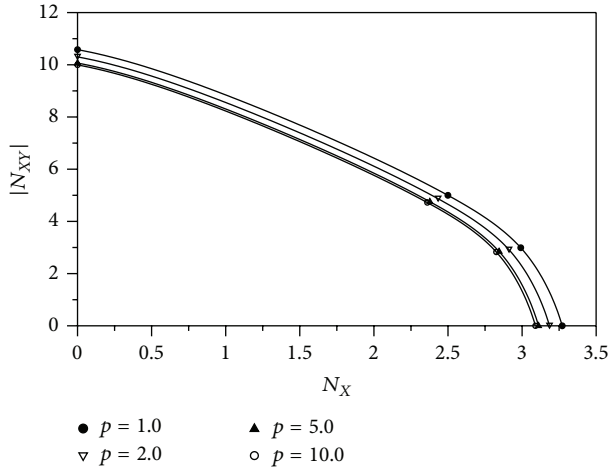

Figure 10: Buckling load of FGM plates with various power law index: combined compressive and shear loading.

when it is subjected to compression. For combined shear and compressive loading the stability envelopes are symmetric about the line N_{xy}.

(4) The suitable selection of sampling point used in ANS method is very important for vibration and buckling behavior of FGM plates. It is noticed that locking phenomenon occurs in the results of reference when the plates become very thin. This phenomenon may lead us to a conclusion that the suitable selection of sampling points prevents the locking problem from occurring in vibration and buckling analysis of either thick FGM plates or very thin ones.

In order to design the FGM plates under the in-plane shear loading, the present formulation and results may serve as benchmark for future guidelines and may be extended to dynamic instability analysis of various FGM structures. The numerical results of present study may serve as benchmark for future guidelines in designing FGM plates under compressive, tension, shear, and combined loading with arbitrary boundary conditions. Also, the present theory should provide engineers with the capability for the design of various FGM plates and shells.

Competing Interests

The author declares that there are no competing interests regarding the publication of this paper.

Acknowledgments

This work was supported by the research grant of the Kongju National University in 2015.

References

[1] Y. L. Chung and S. H. Chi, "The residual stress of functionally graded materials," *Journal of Chinese Institute of Civil and Hydraulic Engineering*, vol. 13, pp. 1–9, 2001.

[2] S.-C. Han, G. R. Lomboy, and K.-D. Kim, "Mechanical vibration and buckling analysis of FGM plates and shells using a four-node quasi-conforming shell element," *International Journal of Structural Stability and Dynamics*, vol. 8, no. 2, pp. 203–229, 2008.

[3] S.-C. Han, W.-H. Lee, and W.-T. Park, "Non-linear analysis of laminated composite and sigmoid functionally graded anisotropic structures using a higher-order shear deformable natural Lagrangian shell element," *Composite Structures*, vol. 89, no. 1, pp. 8–19, 2009.

[4] W.-Y. Jung and S.-C. Han, "Transient analysis of FGM and laminated composite structures using a refined 8-node ANS shell element," *Composites Part B: Engineering*, vol. 56, pp. 372–383, 2014.

[5] Z. Belabed, M. S. Ahmed Houari, A. Tounsi, S. R. Mahmoud, and O. Anwar Bég, "An efficient and simple higher order shear and normal deformation theory for functionally graded material (FGM) plates," *Composites Part B: Engineering*, vol. 60, pp. 274–283, 2014.

[6] A. Hamidi, M. S. A. Houari, S. R. Mahmoud, and A. Tounsi, "A sinusoidal plate theory with 5-unknowns and stretching effect for thermomechanical bending of functionally graded sandwich plates," *Steel and Composite Structures*, vol. 18, no. 1, pp. 235–253, 2015.

[7] W.-H. Lee, S.-C. Han, and W.-T. Park, "A refined higher order shear and normal deformation theory for E-, P-, and S-FGM plates on Pasternak elastic foundation," *Composite Structures*, vol. 122, pp. 330–342, 2015.

[8] S. C. Han, W. T. Park, and W. Y. Jung, "3D graphical dynamic responses of FGM plates on Pasternak elastic foundation based on quasi-3D shear and normal deformation theory," *Composites Part B: Engineering*, vol. 95, pp. 324–334, 2016.

[9] M. L. Bucalem and K. J. Bathe, "High-order MITC general shell elements," *International Journal for Numerical Methods in Engineering*, vol. 36, no. 21, pp. 3729–3754, 1993.

[10] K.-J. Bathe and E. N. Dvorkin, "A formulation of general shell elements—the use of mixed interpolation of tensorial components," *International Journal for Numerical Methods in Engineering*, vol. 22, no. 3, pp. 697–722, 1986.

[11] K. D. Kim and T. H. Park, "An 8-node assumed strain element with explicit integration for isotropic and laminated composite shells," *Structural Engineering and Mechanics*, vol. 13, no. 4, pp. 387–410, 2002.

[12] K. D. Kim, G. R. Lomboy, and S. C. Han, "A co-rotational 8-node assumed strain shell element for postbuckling analysis of laminated composite plates and shells," *Computational Mechanics*, vol. 30, no. 4, pp. 330–342, 2003.

[13] R. H. Macneal and R. L. Harder, "A proposed standard set of problems to test finite element accuracy," *Finite Elements in Analysis and Design*, vol. 1, no. 1, pp. 3–20, 1985.

[14] S.-C. Han, W. Kanok-Nukulchai, and W.-H. Lee, "A refined finite element for first-order plate and shell analysis," *Structural Engineering and Mechanics*, vol. 40, no. 2, pp. 191–213, 2011.

[15] J. C. Simo, D. D. Fox, and M. S. Rifai, "On a stress resultant geometrically exact shell model. Part II: the linear theory; computational aspects," *Computer Methods in Applied Mechanics and Engineering*, vol. 73, no. 1, pp. 53–92, 1989.

[16] O. Polit, M. Touratier, and P. Lory, "A new eight-node quadrilateral shear-bending plate finite element," *International Journal for Numerical Methods in Engineering*, vol. 37, no. 3, pp. 387–411, 1994.